Correlation between Processing Efficiency for Ribonuclease P Minimal Substrates and Conformation of the Nucleotide −1 at the Cleavage Position†

Tilman Zuleeg,‡ Annika Hansen,§ Thomas Pfeiffer,§ Harald Schübel,‡,|| Roland Kreutzer,‡,|| Roland K. Hartmann,§ and Stefan Limmer*,‡,||

Lehrstuhl für Biochemie, Universität Bayreuth, and Ribopharma AG, Universitätsstrasse 30, D-95440 Bayreuth, Germany, and Institut für Biochemie, Medizinische Universität zu Lübeck, Ratzeburger Allee 160, D-23538 Lübeck, Germany

Received July 21, 2000; Revised Manuscript Received November 3, 2000

ABSTRACT: It is demonstrated that acceptor stem duplexes derived from native tRNAs which contain a three-nucleotide extension at the 5′-terminus of mature tRNA are minimal substrates for ribonuclease P from both *Escherichia coli* and *Bacillus subtilis.* Variants with a cytidine at position −1 are most efficiently processed whereas the G −1 variant represents a comparatively poor substrate. An A −1 acceptor stem variant is a slightly better substrate than the G −1 variant though generally distinctly less efficient than the C −1 duplex. This is in qualitative agreement with the frequency of the occurrence of the corresponding nucleotides at position −1 in natural substrates, which is highest for pyrimidines and least for G. NMR analyses of the corresponding acceptor stems reveal that the conformation of the nucleotides at position −1 correlates with the substrate preferences of Ribonuclease P: Whereas C −1 adopts a conformation characterized by a glycosidic angle in the *anti* range (close to high-*anti*), the G −1 is clearly in *syn* conformation, and that of A −1 is intermediate between high-*anti* and *syn*. The riboses of nucleotides −1 are in all cases predominantly 2′-*endo* puckered.

RNase P[1] catalyzes the 5′-maturation of tRNA primary transcripts in all three domains of life (Archaea, Bacteria, and Eukarya) as well as in mitochondria and chloroplasts (*1*). The RNA subunits of RNase P from Bacteria and some Archaea are catalytically active in vitro at elevated salt concentrations in the absence of the RNase P protein components (*2*, *3*). Bacterial RNase P RNAs recognize their substrates by tertiary contacts, except for two to three consecutive Watson−Crick base pairs (*4*−*6*) resulting from interaction of tRNA $_{73}$NCCA$_{76}$ 3′-ends with the L15/16 internal loop (A-type RNase P RNAs, such as *Escherichia coli*) or L15 loop (B-type RNase P RNAs, such as *Bacillus subtilis*).

So far, the smallest model substrate reported to be processed by the *E. coli* RNase P holoenzyme consisted of a 7 base pair acceptor stem helix, a 6 nt 5′-precursor segment and a 3′-ACCA terminus (*7*). Previous studies have shown that such minimal substrates or truncated tRNA derivatives bind with lower affinity to *E. coli* RNase P RNA (*8*, *9*), most likely due to the absence or suboptimal presentation of the T arm of tRNA. For this reason, model substrates of the type shown in Figure 1 strongly depend on recognition elements in the acceptor stem/3′-NCCA module, and losses in binding energy due to the disruption of single contacts cause more severe kinetic defects than in the case of intact precursor tRNA substrates (*10*, *11*). Here we have studied the role of the base identity at position −1 (Figure 1) in the context of an acceptor stem module with a 3 nt 5′-flank. Substrates were

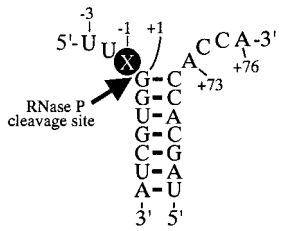

X	*E. coli* holoenzyme k_{obs} (min^{-1})	*B. subtilis* holoenzyme k_{obs} (min^{-1})	*B. subt.* prot. *E. coli* RNA k_{obs} (min^{-1})	*E. coli* prot. *B. sub.* RNA k_{obs} (min^{-1})
C -1	0.40 ± 0.15	1.6 ± 0.2	1.15 ± 0.35	0.05 ± 0.02
A -1	0.18 ± 0.04	(26 ± 5)x10^{-3}	0.24 ± 0.1	(6 ± 2)x10^{-3}
G -1	0.15 ± 0.02	(6.5 ± 2)x10^{-3}	0.14 ± 0.04	(4 ± 3)x10^{-4}

FIGURE 1: Processing rates of acceptor stem model substrates (shown at the top, numbering system as for ptRNAs) by reconstituted bacterial RNase P holoenzymes under single turnover conditions ($E \gg S$; for details see Materials and Methods). Cleavage rates represent mean values derived from two to five independent experiments. We note that the presence of a C, A, or G at position −1 minimized the potential of base pairing between nucleotides −1 and +73. As demonstrated by Lee et al. (*41*) such a base pair formation interferes with substrate positioning in the RNase P active site. In the case of a U at −1 this may be due to introducing an energetic barrier to the interaction of A73 with U294 of *E. coli* RNase P RNA, corresponding to U260 in *B. subtilis* RNase P RNA (*6*, *11*, *38*−*40*).

† This work was supported by the Deutsche Forschungsgemeinschaft, projects Li 722/2-1 and Ha 1672/4-2/4-3.

* To whom correspondence should be adressed. Phone: +49 921 55 2408. Fax: +49 921 55 2432. E-mail: stefan@btc9x3.che.uni-bayreuth.de.

‡ Universität Bayreuth.

§ Medizinische Universität zu Lübeck.

|| Ribopharma AG.

[1] Abbreviations: A, adenosine; *B.s.*, *Bacillus subtilis*; C, cytidine; DSS, 2,2-dimethyl-2-silapentane-5-sulfonate; *E.c.*, *Escherichia coli*; G, guanosine; NMR, nuclear magnetic resonance; ptRNA, precursor tRNA; RNase P, ribonuclease P; X, ribonucleotide (A, C, or G).

10.1021/bi0016974 CCC: $20.00
Published on Web 02/23/2001

analyzed for processing efficiency in reactions catalyzed by reconstituted *E. coli* RNase P and *B. subtilis* RNase P as well as chimeric holoenzymes. Inclusion of chimeric holoenzymes allows to assess if possible differences in cleavage efficiency are primarily related to the nature of the RNA or protein subunit. Little is known about the cleavage efficiency of small model substrates in the reaction catalyzed by *B. subtilis* RNase P, whose catalytic RNA subunit differs from A-type, *E. coli*-like RNase P RNAs significantly in terms of structure (*12*), the mono- and divalent cation concentration required for high catalytic performance in vitro (*2*, *13*, *14*), and the strict requirement for Mg^{2+} or Ca^{2+} in addition to Cd^{2+} for productive interaction with a substrate carrying a single R_p-phosphorothioate modification at the RNase P cleavage site (*15*). Pan (*16*) selected small model substrates for *B. subtilis* RNase P RNA by in vitro selection, providing the first evidence that non-tRNA substrates for RNase P may also exist in *B. subtilis*. The base at position −1 has been shown before to influence cleavage site selection in the *E. coli* RNase P RNA-alone reaction (*17*). The goal of the present study was to determine if there are correlations between the efficiency of bacterial RNase P processing of substrates with different nucleotides at position −1 and structural and/or conformational properties of these variants as determined via NMR spectroscopy.

MATERIALS AND METHODS

RNA Synthesis, Purification, and NMR Sample Preparation. Oligoribonucleotides were chemically synthesized on a Gene Assembler Plus (Pharmacia) by the H-phosphonate method (*18*). Deprotected oligonucleotides were purified by HPLC on a DEAE 500-7 anion-exchange column (Macherey-Nagel). Purification was carried out under denaturing conditions (8 M urea, 20 mM potassium phosphate buffer, 60 °C). Oligoribonucleotides were separated using KCl gradients and subsequently desalted on a P6 column (Bio-Rad). Sample purity was checked by denaturing PAGE (7 M urea). RNA concentrations were determined via UV absorption at 260 nm. NMR samples with final RNA concentrations between ca. 1.0 and 1.3 mM were prepared in D_2O solution containing 100 mM NaCl and 10 mM sodium phosphate, pH 6.5. Samples were annealed by heating to 80 °C for 3 min and subsequent cooling (2−3 h) to room temperature.

NMR Spectroscopy. ^{1}H NMR spectra were acquired at 500 MHz proton resonance frequency on a DRX-500 spectrometer (Bruker) and processed and evaluated on O2 and Indigo^2 workstations (SGI) using the NDEE NMR software (Spinup). All chemical shifts are referenced to internal DSS. One-dimensional spectra were acquired with 10 ppm spectral width and 16 K data points and two-dimensional spectra likewise with 10 ppm sweep width in both dimensions and 4096 × 512 data points ($F_2 \times F_1$). 1D spectra were subjected to exponential multiplication corresponding to 0.5 Hz line broadening (convolution). 2D spectra were apodized with $\pi/2$-shifted squared sine-bell functions in both dimensions. NOESY (mixing times of 80, 150, and 350 ms) and DQF-COSY spectra were recorded in the phase-sensitive mode using standard pulse sequences at temperatures of 289, 297, and 303 K. Heteronuclear ^{13}C−^{1}H correlations were measured as HMQC spectra with GARP decoupling in t_2. The 2048 × 512 ($F_2 \times F_1$) data points were used with spectral widths of 10 ppm for the proton resonances and 130 ppm for the carbon dimension.

Preparation of RNase P RNAs and Proteins. Wild-type RNase P RNAs from *E. coli* and *B. subtilis* were synthesized by in vitro runoff transcription from plasmid DNAs and prepared as described (*15*, *19*). *E. coli* and *B. subtilis* RNase P proteins carrying an N-terminal His tag (His-tagged peptide leader: MRGSHHHHHHGS, encoded in plasmid pQE-30, Qiagen) were expressed and purified as described (*20*), except that protease inhibitors pepstatin and antipain were omitted, and cell disruption was achieved by sonication pulses for 20 min on ice but without repeated freeze−thawing.

Nuclease P1 and Alkaline Hydrolysis Reactions. For limited digests by nuclease P1, about 2 × 10^4 Cerenkov cpm of the RNA oligonucleotide and 2.5 μg of carrier tRNA were preincubated in buffer P1 (40 mM NH_4OAc, pH 5.3, 0.4 mM $ZnSO_4$) for 5 min at 70 °C, followed by addition of 0.001 μg of nuclease P1 (Boehringer) to a final reaction volume of 10 μL and further incubation for 1 min at 70 °C, if not stated otherwise. For limited alkaline hydrolysis, about 2 × 10^4 Cerenkov cpm of the RNA probe and 2.5 μg of carrier tRNA were incubated for 1.5 min at 100 °C in 10 μL of 30 mM NaOH and 0.6 mM EDTA. All hydrolysis reactions were stopped by addition of an equal volume of gel loading buffer (1× TBE buffer containing 2.7 M urea, 66% formamide, and 0.05% each XCB and BPB).

5′-End Labeling of RNA Oligonucleotides. 5′-End labeling using [γ-^{32}P]ATP and T4 polynucleotide kinase was performed as described (*21*).

Kinetics. 5′-^{32}P-end-labeled (about 1 pmol) RNA oligonucleotides 5′-UU(C, A, or G)GGUGCUA were annealed with an about 10^3-fold excess of the complementary RNA oligonucleotide 5′-UAGCACCACCA (about 1 nmol) in 15 μL of buffer A [50 mM HEPES pH 7, 30 mM $Mg(OAc)_2$, 100 mM NH_4OAc] at 92 °C for 3 min, followed by slow cooling (2−3 h) to room temperature.

About 10 fmol (25 000 cpm) of the annealed RNA oligonucleotides was prewarmed for 10 min at 37 °C in buffer A and then combined with 5 μM each RNase P RNA and protein (RNA and protein had been preincubated together for 30 min at 37 °C in buffer A) in a final volume of 15 μL of buffer A. Aliquots (2.5 μL) were taken at different time points, 5 μL of gel loading buffer (see above) was added, and RNAs were separated on 15% or 25% polyacrylamide/7 M urea gels and quantified as described (*15*).

RESULTS

Kinetics. Small bipartite model substrates carrying a 3 nt 5′-flank (Figure 1) were analyzed under single turnover conditions by RNase P holoenzymes reconstituted from RNA and protein components derived from *E. coli* and *B. subtilis*. Under the same conditions (up to 1 h incubation at pH 7.0, 30 mM Mg^{2+}, 0.1 M NH_4^+), processing by *E. coli* RNase P RNA alone was much less efficient, and no detectable cleavage was seen in the presence of *B. subtilis* RNase P RNA alone (data not shown). Figure 2 illustrates a representative gel analysis of the time course of substrate conversion in the presence of the four different holoenzyme activities. In addition, we verified that cleavage occurred between position −1 and +1, as shown for the A −1 and G

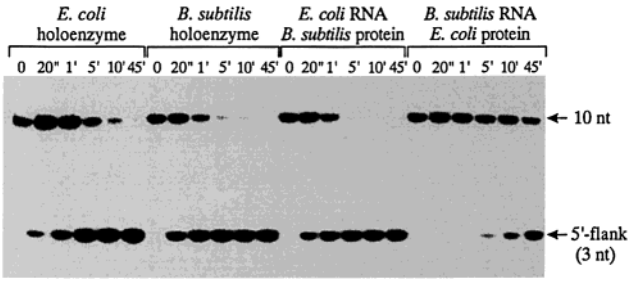

FIGURE 2: Kinetics of cleavage for the acceptor stem model substrate carrying a C at position −1 by reconstituted bacterial RNase P holoenzymes under single turnover conditions ($E \gg S$). Aliquots were withdrawn at indicated time points, and cleavage reactions were analyzed by 25% PAGE in the presence of 7 M urea. The 5′-end-labeled substrate strand, 10 nucleotides in length, and the 5′-cleavage product, 3 nucleotides in length, are indicated by arrows. For further details, see Materials and Methods.

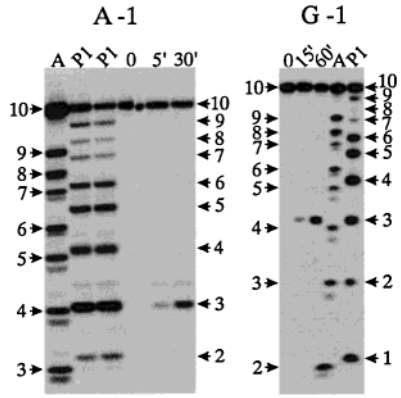

FIGURE 3: Determination of the cleavage site illustrated for the model substrate carrying an A or G at position −1 in the reaction catalyzed by the *E. coli* RNase P holoenzyme. The extent of substrate conversion is shown for two time points. Limited alkaline (OH^-) and nuclease P1 digests are shown for comparison. For the A-1 substrate, two nuclease P1 lanes are shown, which differed in the time of incubation (30 s and 2 min at 70 °C, respectively). Note that alkaline hydrolysis generates 5′-OH and 2′,3′-cyclic phosphates, whereas nuclease P1, as RNase P, generates 5′-phosphate and 3′-OH termini. The 5′-end-labeled substrate oligonucleotides 5′-UU(A or G)GGUGCUA are 10 nucleotides in length. Hydrolysis products were analyzed by 25% PAGE in the presence of 7 M urea. Positions of cleavage products (in nucleotides) for alkaline hydrolysis and nuclease P1 are shown at the left and right margins, respectively. For further details, see Materials and Methods.

−1 substrate in Figure 3. Coelectrophoresis with limited alkaline and nuclease P1 digests also confirmed that RNase P cleavage generated authentic 5′-phosphate termini (Figure 3). Single turnover rates of cleavage (k_{obs}) are summarized in Figure 1 and varied in the range between about 10^{-4} and 1.6 min^{-1}.

In reactions catalyzed by the *E. coli* RNase P holoenzyme, the substrate carrying a cytidine at position −1 was processed at the highest rate, although the two other substrates were cleaved with only slightly reduced (2.2−2.7-fold) efficiencies. A different picture emerged with holoenzymes including the *B. subtilis* RNA component. In these cases, the C −1 substrate was cleaved 62-fold faster than the A −1 substrate with the *B. subtilis* holoenzyme and about 8.3-fold faster in the presence of the *B. subtilis* RNA and *E. coli* protein (*B.s.* RNA/*E.c.* protein enzyme). This difference reduced to 4.8-fold with the *B.s.* protein/*E.c.* RNA enzyme. In all cases, lowest processing efficiencies were observed with the G −1

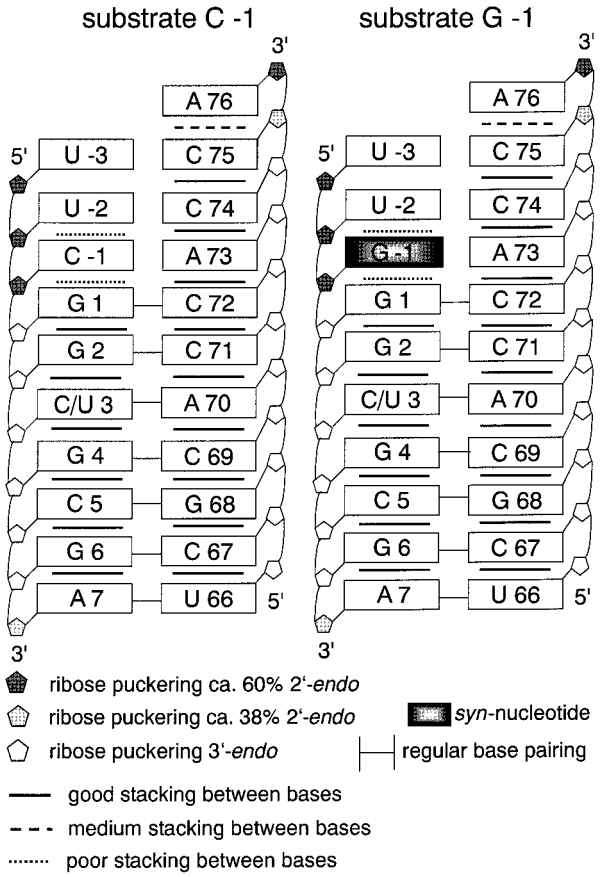

FIGURE 4: Schematic representation of stacking interactions and nucleotide conformations in minimal substrates C −1 and G −1 as derived from NMR studies. Base stacking interactions were classified as "good", "medium", and "poor" according to the number and intensity of characteristic internucleotide NOESY cross-peaks. Additional C3 variants were used for comparison to verify the assignment of the stem nucleotides (*22*, *42*, *43*).

substrate, although the differences to the A −1 substrate were relatively moderate for activities containing the *E. coli* RNA component (1.2−1.7-fold), more pronounced for the *B. subtilis* holoenzyme (4-fold), and most pronounced for the combination *E.c.* protein/*B.s.* RNA (15-fold). These results indicate that a purine at −1 is generally less favorable for productive enzyme−substrate interaction than a pyrimidine. However, enzymes containing the *E. coli* RNA component were only moderately sensitive to the base identity at position −1, whereas those containing the *B. subtilis* RNA component were more sensitive; these observations indicate that active site constraints are not identical for enzyme−substrate complexes involving the two different catalytic RNAs.

NMR Analysis. In our NMR studies, minimal RNA substrates for RNase P were employed that resemble the acceptor stem of *E. coli* $tRNA^{Ala}$ (Figure 1). In all cases, the 5′-flank of the mature tRNA acceptor stem was extended by a 3 nt stretch, 5′-UUX, where X denotes one of the nucleotides C, G, or A at position −1. U −1 was purposefully excluded to avoid base pair formation between U −1 and A73 (see further explanation in the legend of Figure 1).

General Features of the Acceptor Stem Structures with 5′-UUX Overhangs. The general features are schematically depicted in Figure 4 for the C −1 and G −1 variants, respectively. As in the wild-type acceptor stem of $tRNA^{Ala}$ (*22*), the 4 nt single-stranded 3′-terminus (ACCA) also

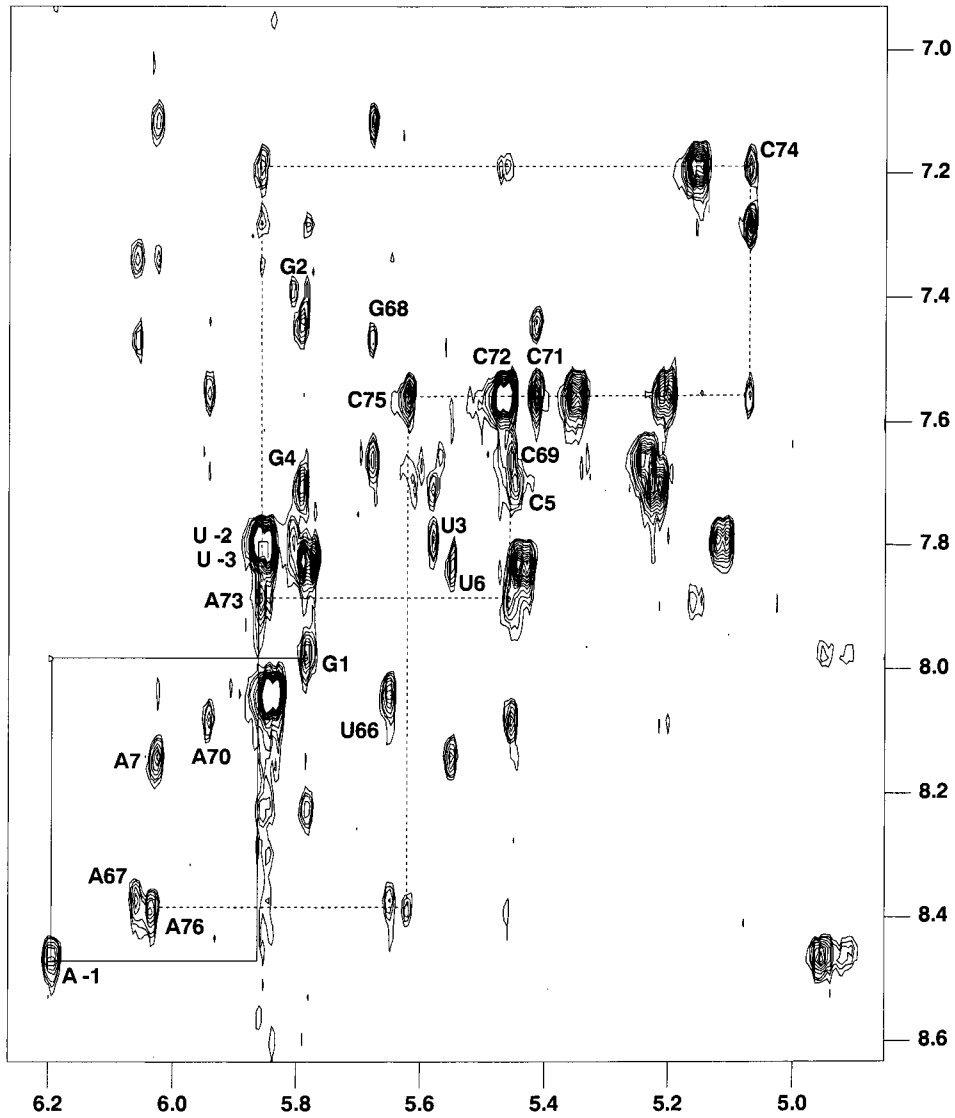

FIGURE 5: Part of the 350 ms NOESY spectrum at 297 K of the A −1 variant containing the H1′/H5↔H6/H8 cross-peak region. Assignment paths are indicated for nucleotides U −3 through G1 (5′-terminus, solid lines) and nucleotides C72 through A76 (3′-terminus, dashed lines).

displayed a fairly high degree of conformational order in these duplex variants, i.e., nucleotides A73 through C75 are well-stacked, with the terminal A76 being less ordered, and accordingly featuring greater reorientational freedom. The number and strength of internucleotide NOEs between the corresponding nucleotides are comparable to those between the residues in the interior of the double helical stem (*22*−*25*). In particular, very strong NOEs are observed between the ribose H2′ resonance of a given nucleotide and the aromatic (H6/H8) proton signal of the base of its 3′-neighbor for nucleotides 66 through 76 in the one strand and 1 through 7 in the other strand. Moreover, strong intranucleotide ribose H3′↔aromatic H6/H8 contacts (except for A76 where a very strong intranucleotide H2′↔H8 NOESY cross-peak was observed) were found for these residues, as well as weak to medium ribose H1′↔aromatic H6/H8 NOESY cross-peaks (both intra- and internucleotide) and weak aromatic−aromatic (H6/H8↔H6/H8, H5↔H5, H6↔H5) internucleotide contacts. Such a cross-peak pattern, along with the observed preferential 3′-*endo* puckering of all nucleotide riboses (except for A76 which has a 2′-*endo* population of about 57%; cf. Figure 4), indicates an essentially regular A-helical geometry (*24*−*28*). Addition of 8 mM $MgCl_2$ gives rise to only minor chemical shift changes (typically <0.03 ppm), while cross-peak pattern as well as relative cross-peak intensities remained unaffected (data not shown).

The results were distinctly different for the three nucleotides −3 to −1 in the 5′-flank of the 5′-terminus of the tRNA acceptor stem. Irrespective of the nature of the nucleotide type at position −1, the riboses of all three nucleotides were predominantly 2′-*endo* puckered [ca. 57%; see (*29*)]. This already hints at an arrangement of the nucleotides in the overhang which clearly deviates from regular A-geometry that requires 3′-*endo* puckering of the ribose rings. Moreover, all studied minimal substrates have in common that there are only very weak NOE contacts between nucleotides U −3 and U −2, suggesting strongly diminished stacking between them and concomitantly high reorientational freedom. In Figure 5, part of the 350 ms NOESY spectrum of the A −1 variant containing the H1′/H5↔H6/H8 cross-peaks is displayed. Assignment paths connecting nucleotides U −3 through G1 of the 5′-extension (solid lines) and nucleotides C72 through A76 (dashed lines) are drawn. It is obvious that several internucleotide H1′↔H6/H8 cross-peaks are either

very weak or completely absent in the former case. In the latter case, internucleotide cross-peaks are clearly present, reflecting the well-ordered arrangement (stacking) of the nucleotides in the 3′-terminal ACCA end. There were only very weak (if any) H2′↔aromatic H6 internucleotide cross-peaks for the 5′-terminal nucleotides, indicating that the arrangement in this region of the RNA is distinctly different from regular A-helical conformation. In line with the preferred 2′-*endo* pucker of the riboses of U −3 and U −2 (as derived from the relatively large $J^{H1'H2'}$ scalar coupling constants of 4.9 Hz), very strong intranucleotide H2′↔H6 cross-peaks were detected for these nucleotides, which is more typical of B-like helices (*24*−*26*). Hence, we infer that the reorientational freedom of this arrangement is rather high or, correspondingly, the conformational order (along with the stacking order of the bases) is fairly low. This inference is corroborated by the magnitudes of the chemical shifts of both the aromatic (H5/H6) and ribose H1′ protons of U −3 and U −2, which were closer to the values expected for nucleotides in totally disordered ("coiled") RNA single strands (*30*). If significant stacking between the bases occurred, these resonances would be appreciably shifted upfield (*30*), which was not the case. Noticeable differences with respect to nucleotide conformation and internucleotide contacts between the variants with different bases at position −1 are essentially restricted to this nucleotide and others in its immediate vicinity (see below).

Base-Type-Dependent Conformational Peculiarities at Position −1. For all acceptor stem minimal substrates with variant nucleotides at position −1 (C, A, G), NOE contacts between nucleotides U −2 and X −1 were generally very weak without significant differences regarding the cross-peak pattern. However, distinct variations were found with respect to the interaction between nucleotide X −1 and G1. For the C −1 duplex (see above), again very weak internucleotide contacts C −1H1′↔G1H8 and C −1H2′↔G1H8 were observed, whereas the intranucleotide C −1 H2′↔H6 cross-peak was by far the strongest. Moreover, a weak U −2H2′↔C −1H5 cross-peak was seen (cf. Figure 6). Along with the preferential 2′-*endo* puckering of its ribose this is in accordance with the assumption of a somewhat modified "B-like" arrangement of C −1 (with reference to its neighbors) which in addition displayed a high degree of conformational disorder.

Variants with A −1 (cf. Figure 5) and G −1 likewise featured only very weak A/G −1H1′↔G1H8 cross-peaks; however, in these cases the internucleotide A/G −1H2′↔G1H8 contacts were weak to medium, i.e., comparatively stronger than the equivalent ones for the C −1 variant (see Figure 6).

Most significantly, the C −1 and G −1 variants differed in the relative intensities of intranucleotide H1′↔H6/H8 and H2′↔H6/H8 cross-peaks. Though, due to peak overlap with the C −1H5↔H6 cross-peak, the intranucleotide C −1H1′↔H6 cross-peak was not resolvable, however, its intensity could be estimated from the total intensity of the resulting superimposed cross-peak and its comparison with other H5↔H6 cross-peaks. From this comparison it could be inferred that the H1′↔H6 cross-peak of C −1 was not extraordinarily strong. As discussed before, in the C −1 substrate the intranucleotide H2′↔H6 cross-peak is the strongest one (cf. Figure 6), much more intense than any other contact involving resonances of C −1. For the G −1 variant, however, a very strong intranucleotide G −1H1′↔H8 cross-peak is observed. Its intensity clearly exceeded that of all other contacts between G −1 resonances and those of its neighboring nucleotides as well as that of its intranucleotide cross-peaks, in particular, the G −1H2′↔H8 intranucleotide and the G −1H2′↔G1H8 internucleotide contacts (see Figure 6). The G −1H1′↔H8 intranucleotide cross-peak was still observed in the NOESY spectrum at short mixing time (80 ms), while all other cross-peaks involving resonances from G −1 are missing in this spectrum.

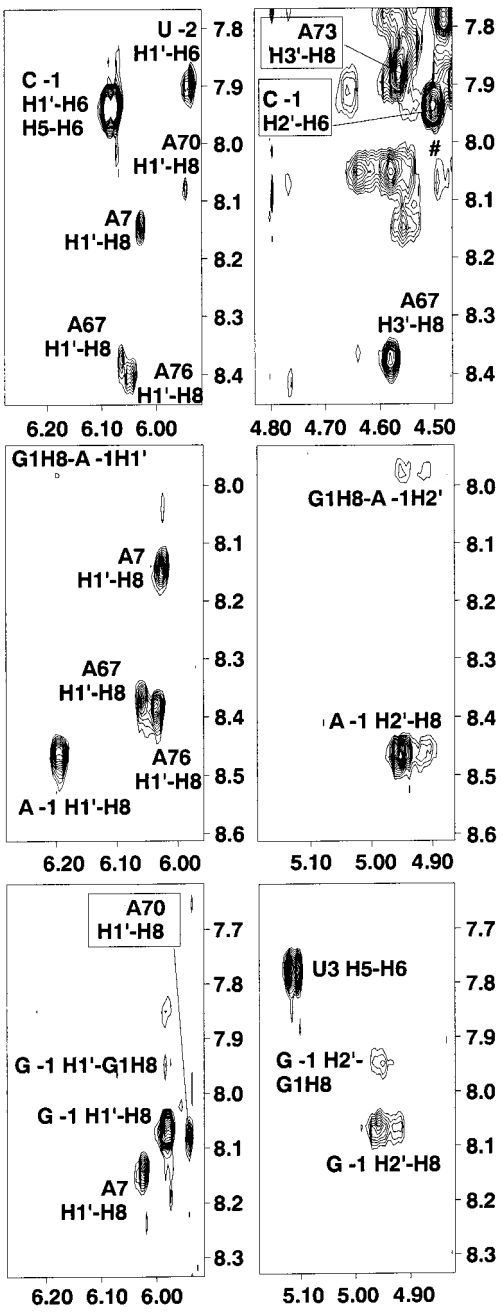

FIGURE 6: Part of the 350 ms NOESY spectra at 297 K of the C −1 (upper panel), A −1 (middle panel), and G −1 (lower panel) minimal substrates for RNase P containing the intranucleotide A −1/C −1/G −1 H1′↔H8/H6 and H2′↔H8/H6 cross-peaks, respectively. Note their different relative intensity ratios (cf. Results). (#) indicates the missing internucleotide G1′H8↔C −1H2′ cross-peak (cf. Results).

Very strong intranucleotide H1′↔H8 cross-peaks are usually taken as evidence of a *syn* conformation of the corresponding nucleotide (*24*−*27*, *31*−*33*). This conformation was further corroborated by the downfield-shifted H2′ resonance of G −1 (4.95 ppm), which is typical of *syn* nucleotide H2′ shifts (*28*, *32*) though it is not as pronounced here as in other reports (*32*). Consistent with a *syn* conformation of G −1 was the detection of a weak internucleotide G −1H2′↔G1H8 cross-peak, which is comparatively stronger than the equivalent C −1H2′↔G1H8 in the C −1 variant ("B-like" arrangement). From the relative intensities of the above-discussed cross-peaks, a rough estimate for the glycosidic angle χ of ca. 0° (±20°) can be assigned (*24*).

Interestingly, the C −1 variant had a rather unusual cross-peak between resonances of the two first nucleotides in either of the two single-strand termini on the 5′- and 3′-ends of the precursor, respectively, namely C −1H5↔A73H2 (weak to medium). Such a cross-peak, though much more intense there, has been also observed between C1H5↔A72H2 of the nucleotides in the characteristic first mismatch base pair C1·A72 of the *E. coli* initiator $tRNA^{fMet}$ acceptor stem (*34*). In that molecule, for nucleotide C1, from the NMR structure analysis, a conformation close to high-*anti* (glycosidic angle $\chi \approx -100°$) was derived. In the present case, the arrangement is evidently much less well defined due to increased conformational flexibility. Nevertheless, there seems to be a certain probability of finding the corresponding glycosidic angle χ close to the high-*anti* range.

Remarkably, the adenosine in the A −1 variant appears to adopt a conformation being somehow intermediate between those of C −1 and G −1 minimal substrates. The NOESY spectra of A −1 displayed medium to strong intranucleotide H1′↔H8 cross-peaks, which are invariably distinctly less intense than the strong A −1 H2′↔H8 intranucleotide contacts (cf. Figure 6). Internucleotide A −1H2′↔G1H8 cross-peaks (weak) were comparatively stronger than the corresponding C −1H2′↔G1H8 contacts for the C −1 variant, very much like for the G −1 acceptor stem. In addition, weak to medium A −1H2↔G1H1′ and very weak A −1H1′↔G1H8 cross-peaks suggest some residual stacking between A −1 and G1.

Possibly, A −1 switches rapidly (on the NMR time scale) between *syn* and *anti* conformations and/or had a preferred occupation between high-*anti* and *syn* regions. An estimated average glycosidic angle χ of ca. $-50° \pm 20°$ can account for all the observed cross-peak patterns (see above; cf. also Figure 6).

DISCUSSION

Acceptor stem model substrates carrying a 3 nt 5′-flank have been analyzed in reactions catalyzed by reconstituted *E. coli* RNase P and *B. subtilis* RNase P as well as chimeric holoenzymes (Figure 1). These substrates represent the smallest truncated tRNA substrates tested to date, and our study is the first data on their cleavage by a bacterial enzyme of the B-type, for which *B. subtilis* has previously been the prototype. Our results suggest that *B. subtilis* RNase P, as the *E. coli* enzyme (*35*), may also act on non-tRNA substrates in vivo, which include a single-stranded 5′-flank, an acceptor stem-like module, and a single-stranded 3′-NCCA terminus. Pan (*16*) even obtained by in vitro selection small model substrates for *B. subtilis* RNase P RNA that are cleaved in an apparently single-stranded region and do not depend on the presence of a 3′-NCCA terminus, raising the possibility that the scope of natural RNase P substrates might be unexpectedly diverse. However, non-3′-NCCA substrates could contain features that significantly impair cleavage. Some precursors are more efficiently processed by the holoenzyme than by the RNA subunits alone (*7*, *36*). Fierke and co-workers (*37*) have reported evidence that the *B. subtilis* protein component stabilizes productive interactions of the catalytic RNA subunit with the substrate in a manner dependent on the presence of nucleotide −2 in the precursor segment. Kinetic and cross-linking experiments further indicated that the protein component increases the substrate association rate by directly interacting with nucleotide −5 of the precursor segment (*6*, *11*, *38*−*40*). Since the substrates analyzed here had only a 3 nt 5′-flank, the protein most likely acted indirectly by stabilizing productive interactions between catalytic RNA subunits and small model substrates.

Holoenzymes containing *B. subtilis* RNase P RNA were most sensitive to a purine, particularly G, at position −1 of the substrate. This is in line with a previous study showing that changing a 2 nt 5′-flank from 5′-GU to GG in the context of a bacterial $ptRNA^{Asp}$ decreased the cleavage rate constant about 70-fold in the reaction catalyzed by *B. subtilis* RNase P (*37*). In our study, the C −1 substrate was cleaved about 250- and 125-fold faster than the G −1 substrate by the *B. subtilis* holoenzyme and the *B.s.* RNA/*E.c.* protein chimeric enzyme, respectively, suggesting that these differences may include contributions from impaired substrate binding in the ground state in addition to reducing the rate of the cleavage step. A comparative analysis of naturally occurring *B. subtilis* ptRNA leader sequences revealed little sequence conservation, except that the nucleotide at position −1 is predominantly U and most rarely G (*37*), with the latter finding being consistent with our observed in vitro result reported above. A similar bias is observed for *E. coli*, where about 67% of tRNA precursors carry a U and only about 15% a purine at position −1 (*40*). However, our results (Figure 1) indicate that the catalytic RNA subunit from *E. coli* has only moderate preference for a pyrimidine at position −1.

Our NMR measurements have revealed that nucleotides in the 5′-precursor segment display only little stacking order and, accordingly, high reorientational freedom in free substrates, in contrast to the well-ordered 3′-terminus. As discussed above, the first two nucleotides of the 5′-flank are assumed to be involved in interactions with the catalytic RNA subunit, suggesting that precursor fragments will adopt a more defined, yet unknown, conformation in RNase P−substrate complexes. With the C −1 substrate, the nucleotide at this position adopts the *anti* conformation, though it might be close to the high-*anti* range. A rapid exchange on the NMR time scale between *syn* and *anti* conformers at this position seems probable for the A −1 substrate (although we do not exclude an average conformation intermediate between high-*anti* and *syn* with the glycosidic angle χ around −50°) whereas a guanosine −1 shifts this equilibrium toward the *syn* conformation. If this conformational equilibrium was the main determinant in formation of productive enzyme−substrate complexes, we would have expected the A −1 substrate to result in cleavage efficiencies intermediate between the C −1 and G −1 substrate. This was indeed

observed for the *E. coli* holoenzyme. However, the differences between the C −1 versus the A −1, G −1 substrates were much more pronounced than for the A −1 versus the G −1 substrate in the reaction catalyzed by the *B. subtilis* holoenzyme. However, the binding preferences need not necessarily be conserved in various systems.

Thus, the *anti*/*syn* conformational equilibrium could play a role in the recognition process by bacterial RNase P by virtue of reducing the frequency of successful initial binding events. However, other reasons may be the primary cause for the observed kinetic effects. A more bulky purine at −1 might prevent an optimal alignment of the scissile phosphodiester bond in the active site, particularly in enzyme−substrate complexes containing the *B. subtilis* RNase P RNA.

ACKNOWLEDGMENT

We thank Christopher J. Green for providing the pQE-30 plasmids encoding *E. coli* and *B. subtilis* RNase P proteins and Rita Held for excellent technical assistance.

REFERENCES

1. Frank, D. N., and Pace, N. R. (1998) *Annu. Rev. Biochem. 67*, 153−180.
2. Guerrier-Takada, C., Gardiner, K., Marsh, T., Pace, N., and Altman, S. (1983) *Cell 35*, 849−857.
3. Pannucci, J. A., Haas, E. S., Hall, T. A., Harris, J. K., and Brown, J. W. (1999) *Proc. Natl. Acad. Sci. U.S.A. 96*, 7803−7808.
4. Kirsebom, L. A., and Svärd, S. G. (1994) *EMBO J. 20*, 4870−4876.
5. Svärd, S. G., Kagardt, U., and Kirsebom, L. A. (1996) *RNA 5*, 463−472.
6. Tallsjö, A., Kufel, J., and Kirsebom, L. A. (1996) *RNA 4*, 299−307.
7. Forster, A. C., and Altman, S. (1990) *Science 249*, 783−786.
8. Schlegl, J., Fürste, J. P., Bald, R., Erdmann, V. A., and Hartmann, R. K. (1992) *Nucleic Acids Res. 20*, 5963−5970.
9. Hardt, W.-D., Schlegl, J., Erdmann, V. A., and Hartmann, R. K. (1993) *Biochemistry 32*, 13046−13053.
10. McClain, W. H., Guerrier-Takada, C., and Altman, S. (1987) *Science 238*, 527−530.
11. Svärd, S. G., and Kirsebom, L. A. (1992) *J. Mol. Biol. 227*, 1019−1031.
12. Haas, E. S., Banta, A. B., Harris, J. K., Pace, N. R., and Brown, J. W. (1996) *Nucleic Acids Res. 24*, 4775−4782.
13. Guerrier-Takada, C., Haydock, K., Allen, L., and Altman, S. (1986) *Biochemistry 25*, 1509−1515.
14. Reich, C., Olsen, G. J., Pace, B., and Pace, N. R. (2000) *Science 239*, 178−181.
15. Warnecke, J. M., Held, R., Busch, S., and Hartmann, R. K. (1999) *J. Mol. Biol. 290*, 433−445.
16. Pan, T. (1995) *Biochemistry 34*, 8458−8464.
17. Krupp, G., Kahle, D., Vogt, T., and Char, S. (1991) *J. Mol. Biol. 217*, 637−648.
18. Ott, G., Arnold, L., Smrt, J., Sobkowski, M., Limmer, S., Hofmann, H.-P., and Sprinzl, M. (1994) *Nucleosides Nucleotides 13*, 1069−1085.
19. Hardt, W. D., and Hartmann, R. K. (1996) *J. Mol. Biol. 259*, 422−433.
20. Rivera-Leon, R., Green, C. J., and Vold, B. S. (1995) *J. Bacteriol. 177*, 2564−2566.
21. Heide, C., Pfeiffer, T., Nolan, J. M., and Hartmann, R. K. (1999) *RNA 5*, 102−116.
22. Vogtherr, M., and Limmer, S. (1998) *FEBS Lett. 433*, 301−306.
23. Ramos, A., and Varani, G. (1997) *Nucleic Acids Res. 25*, 2083−2090.
24. Wüthrich, K. (1986) *NMR of Proteins and Nucleic Acids*, John Wiley & Sons, New York.
25. Wijmenga, S. S., Mooren, M. M. W., and Hilbers, C. W. (1993) in *NMR of Macromolecules: A Practical Approach* (Roberts, G. C. K., Ed.) pp 217−288, IRL Press, Oxford.
26. Goljer, I., and Bolton, P. H. (1994) in *Two-Dimensional NMR Spectroscopy* (Croasmun, W. R., and Carlson, R. M. K., Eds.) pp 699−740, VCH Wiley, New York, Weinheim, and Cambridge.
27. Varani, G., Aboul-ela, F., and Allain, F. H. T. (1996) *Prog. NMR Spectrosc. 29*, 51−127.
28. Wijmenga, S. S., and van Buuren, B. N. M. (1998) *Prog. NMR Spectrosc. 32*, 287−387.
29. Altona, C. (1982) *Rec. Rev. Prog. Curr. Res. 101*, 413−433.
30. Hader, P. A., Alkema, D., Bell, R. A., and Neilson, T. (1982) *J. Chem. Soc., Chem. Commun.*, 10−12.
31. Peterson, R. D., and Feigon, J. (1996) *J. Mol. Biol. 264*, 863−877.
32. Jiang, F., Fiala, R., Live, D., Kumar, R. A., and Patel, D. J. (1996) *Biochemistry 35*, 13250−13266.
33. Butcher, S. E., Dieckmann, T., and Feigon, J. (1997) *EMBO J. 16*, 7490−7499.
34. Zuleeg, T., Vogtherr, M., Schübel, H., and Limmer, S. (2000) *FEBS Lett. 472*, 247−253.
35. Schön, A. (1999) *FEMS Microbiol. Rev. 23*, 391−406.
36. Liu, F., and Altman, S. (1994) *Cell 77*, 1093−1100.
37. Crary, S. M., Niranjanakumari, S., and Fierke, C. A. (1998) *Biochemistry 37*, 9409−9416.
38. Kirsebom, L. A., and Svärd, S. G. (1992) *Nucleic Acids Res. 20*, 425−432.
39. Brannvall, M., and Kirsebom, L. A. (1999) *J. Mol. Biol. 292*, 53−63.
40. Kufel, J., and Kirsebom, L. A. (1996) *Proc. Natl. Acad. Sci. U.S.A. 93*, 6085−6090.
41. Lee, Y., Kindelberger, D. W., Lee, J.-Y., McLennen, S., Chamberlain, J., and Engelke, R. (1997) *RNA 3*, 175−185.
42. Gabriel, K., Schneider, J., and McClain, W. H. (1996) *Science 271*, 195−197.
43. Limmer, S., Reif, B., Ott, G., Arnold, L., and Sprinzl, M. (1996) *FEBS Lett. 385*, 15−20.

BI0016974